國立臺灣大學理學院物理學系

碩士論文

Department of Physics

College of Science

National Taiwan University

Master's Thesis

以蒙地卡羅法尋找Belle ll實驗中B介子至ϕK_L^0介子之衰變事件

MC study for $B^0 \rightarrow \phi K_L^0$ decay at Belle ll

林偉哲

Wei-Che Lin

指導教授：王名儒 教授

Advisor: Min-Zu Wang, Ph.D.

中華民國 114 年 2 月

February 2025

doi:10.6342/NTU202500482

doi:10.6342/NTU202500482

國立臺灣大學碩士學位論文
口試委員會審定書
MASTER'S THESIS ACCEPTANCE CERTIFICATE
NATIONAL TAIWAN UNIVERSITY

以蒙地卡羅法尋找 Belle II 實驗中 B 介子至

ϕ K0L 介子衰變事件

MC Study for $B^0 \rightarrow \phi$ K0L decay at Belle II

本論文係____林偉哲__R08222076__在國立臺灣大學_物理所_完成之碩士學位論文，於民國__114_年_01___月_20_日承下列考試委員審查通過及口試及格，特此證明。

The undersigned, appointed by the Department / Institute of Physics on 20 (date) 1 (month) 2025 (year) have examined a Master's thesis entitled above presented by 林偉哲 (name) R08222076 (student ID) candidate and hereby certify that it is worthy of acceptance.

口試委員 Oral examination committee:

王名儒

（指導教授 Advisor）

張寶棣　徐靜戈　張敏娟

doi:10.6342/NTU202500482

誌謝

不知不覺也來到寫下感謝的這一天了! 回首我的台大生涯，有苦也有樂，何其有幸能在台大高能組認識你們!

首先我要向我的指導教授王名儒老師，獻上最誠摯的感謝! 感謝王老師指引我踏入高能物理學的殿堂。在我遇到實驗上的困惑時，只要輕敲 526 的房門，都能獲得老師不厭其煩地指點，使我能朝著一個固定的方向前行!

感謝趙元老師和徐靜戈老師在每週會議上的建議與指點。其中我要特別感謝徐老師! 你總是熱誠地解答我的疑惑，不論是親自花上數十分鐘和我指導，或是在信件中熱心地回復問題!

感謝昱潭在我剛入研究室的階段，提供我有關貝爾實驗和作業系統指令操作的知識。在後期的研究階段，與你的討論總是令我收穫良多!

感謝鉦皓在我還是新人的時候，指導有關分析軟體的操作與知識，讓我能夠逐漸地對研究上手!

感謝彥宇在程式上的指導! 你總是不藏私地分享程式碼，並預先提點我在跑程式或輸入指令時，需要注意的所有重點。有了你的幫助，讓我的研究進度不因技術層面而放緩!

感謝傳彧在高能實驗方法上的幫助! 你總是能用淺白易懂卻切中關鍵的方式，幫助我解開心中的困惑!

感謝 519 的傑澄、文翊、勁豪、瑋承、舟晗、侑澄、柏誠、承軒在各方面大大小小的幫助!

最後也是最重要的，我要感謝最親愛的父母! 感謝我的媽媽，在我感到壓力、

doi:10.6342/NTU202500482

疲累、沮喪時，總是耐心地傾聽我的內心，妳的話語給了我鼓勵與力量! 感謝我的爸爸，無條件地支持我一路完成念物理這個從高中開始的夢想! 你們是我最堅強的後盾!

doi:10.6342/NTU202500482

摘要

本研究探討了 B 介子的潛在衰變模式 $B^0 \to \phi K_L^0$。研究分析了積分亮度為 699.235 fb^{-1} 的蒙地卡羅樣本，以模擬由 SuperKEKB 加速器產生的正子電子對碰撞事件。應用訓練過的多變量分析（MVA）分類器來有效區分 K_L^0 介子與背景噪音。而為了完成信號事件的重建，我們添加了特定的限制條件。在積分亮度為 365.29 fb^{-1} 下，我們得到的信號產量為 137 ± 36。

關鍵字： Belle II 實驗、B 介子、B 衰變、蒙地卡羅方法、超級 B 介子工廠、長命 K 介子

doi:10.6342/NTU202500482

doi:10.6342/NTU202500482

Abstract

This study investigates the potential decay mode $B^0 \to \phi K_L^0$ of B mesons. The research analyzes 699.235 fb^{-1} Monte-Carlo samples to simulate $e^+ e^-$ collisions produced by the SuperKEKB accelerator. A trained multivariate analysis (MVA) classifier is applied to effectively distinguish K_L^0 from background noise. Specific constraints are added to fulfill the reconstruction of signal events. The resulting signal yields are 137 ± 36 under luminosity 365.29 fb^{-1}.

Keywords: Belle II, B meson, B decay, Monte-Carlo method, SuperKEKB, K_L^0

doi:10.6342/NTU202500482

doi:10.6342/NTU202500482

Contents

doi:10.6342/NTU202500482

doi:10.6342/NTU202500482

doi:10.6342/NTU202500482

doi:10.6342/NTU202500482

List of Figures

doi:10.6342/NTU202500482

doi:10.6342/NTU202500482

List of Tables

doi:10.6342/NTU202500482

doi:10.6342/NTU202500482

Chapter 1

Introduction

1.1 The Standard Model

The Standard Model (SM) of particle physics describes our understanding of the most fundamental constituents of nature (the elementary particles) and their interactions. Elementary particles can be classified into three main categories: spin-1/2 *fermions*, spin-1 *gauge bosons*, and spin-0 *Higgs boson*[1].

Fermions, which serve as the fundamental building blocks of nature, consist of *leptons* and *quarks*. Both leptons and quarks are categorized into three generations. Table 1.1 is the summary of the twelve fundamental fermions[2].

Interactions between fundamental fermions are mediated by the gauge bosons. Electromagnetic force is carried out by the massless *photon*. *Gluons* are the force-mediating bosons in strong interaction. In weak charged current reactions, the $W^+$and W^- bosons, with a mass of 80.4 GeV, take responsibility. The neutral Z^0 bosons (M_Z = 91.2 GeV) mediate interactions in the weak neutral current process.

doi:10.6342/NTU202500482

Fermions listed in Table 1.1 can participate in the weak interaction. Except for the electric neutral neutrinos, all other fundamental fermions can interact electromagnetically. Only quarks can participate in strong interactions since they possess color charges.

The bound states of quarks are referred to as *hadrons*. There are two classes of hadrons : *baryons* and *mesons*. Baryons are bound states of three quarks (qqq) or antiquarks ($\overline{q}\,\overline{q}\,\overline{q}$), while mesons are $q\overline{q}$ bound states.

	leptons			quarks		
	particle	charge/e	mass/GeV	particle	charge/e	mass/GeV
first generation	ν_e	0	$< 10^{-9}$	u	+2/3	0.0025
	e^-	-1	0.0005	d	-1/3	0.005
second generation	ν_μ	0	$< 10^{-9}$	c	+2/3	1.3
	μ^-	-1	0.106	s	-1/3	0.1
third generation	ν_τ	0	$< 10^{-9}$	t	+2/3	174
	τ^-	-1	1.78	b	-1/3	4.5

Table 1.1: Fundamental fermions

doi:10.6342/NTU202500482

1.2 Motivation

1.2.1 Mixing of neutral kaons

Neutral kaon states K^0 ($d\bar{s}$) and $\overline{K}^0$ ($s\bar{d}$) can be converted to each other by exchange of two W bosons. If CP is conserved, the observed states are superposition of them

$$
\begin{aligned}
|K_1^0\rangle &= \frac{1}{\sqrt{2}}[|K^0\rangle + |\overline{K}^0\rangle], \\
|K_2^0\rangle &= \frac{1}{\sqrt{2}}[|K^0\rangle - |\overline{K}^0\rangle].
\end{aligned} \tag{1.1}
$$

with CP eigenstates

$$
\begin{aligned}
\hat{C}\hat{P}\,|K_1^0\rangle &= +1\,|K_1^0\rangle \quad (\text{CP even}), \\
\hat{C}\hat{P}\,|K_2^0\rangle &= -1\,|K_2^0\rangle \quad (\text{CP odd}).
\end{aligned} \tag{1.2}
$$

However, since there is evidence of small deviations from CP invariance, the physical states we observed are

$$
\begin{aligned}
|K_S^0\rangle &= \frac{1}{\sqrt{1+|\varepsilon|^2}}[|K_1^0\rangle + \varepsilon\,|K_2^0\rangle], \\
|K_L^0\rangle &= \frac{1}{\sqrt{1+|\varepsilon|^2}}[|K_2^0\rangle + \varepsilon\,|K_1^0\rangle],
\end{aligned} \tag{1.3}
$$

where $|\varepsilon| = (2.228 \pm 0.011) \times 10^{-3}$ is a small factor to describe CP violation in mixing [1][3].

The mass differences between these two states are $m_{K_L^0} - m_{K_S^0} = (3.4839 \pm 0.0059) \times 10^{-12}$ MeV/c^2, whereas the mean lifetimes are $\tau_{K_S^0} = (8.954 \pm 0.004) \times 10^{-11}$ s and $\tau_{K_L^0} = (5.116 \pm 0.021) \times 10^{-8}$ s, respectively [3].

doi:10.6342/NTU202500482

1.2.2 $B^0 \to \phi K^0$ decay

B decays such as $B^0 \to \phi K^0$, which involves b→s$\bar{s}$s transition, are not allowed via first order tree diagrams. However, they can still occur through the higher-order penguin or box ones [4]. Given that $|K^0\!> \approx \frac{1}{\sqrt{2}}[|K_S^0\!> + |K_L^0\!>]$ and the branching fraction $Br(B^0 \to \phi K^0) = (9.0^{+2.2}_{-1.8} \pm 0.7) \times 10^{-6}$ [4], we assume $Br(B^0 \to \phi K_L^0) = 4.5 \times 10^{-6}$.

1.2.3 CP violation in interference

CP violation in mixing contributes a small part to the total decay rates of B mesons. Nonetheless, the decay mode in this study ($B^0 \to \phi K_L^0$) belongs to the rare channels in which B^0 and $\overline{B}^0$ end up to the same final state. The interference between $B^0(\overline{B}^0) \to \overline{B}^0$ (B^0) $\to$ final state and those without mixing will give rise to another kind of CP violation called *CP violation in interference* [1]. Define the asymmetry

$$A \equiv \frac{Prob[\overline{B}^0(t) \to f] - Prob[B^0(t) \to f]}{Prob[\overline{B}^0(t) \to f] + Prob[B^0(t) \to f]}, \tag{1.4}$$

where each *Prob* term denotes the probability that a B^0 or $\overline{B}^0$ at t=0 decays to final state f at time t (oscillation of flavor may occurs). Thus, if we ignore the contribution from direct CP violation, 1.4 becomes

$$A = -\lambda \sin(2\phi_1)\sin(\Delta \mathrm{m} t). \tag{1.5}$$

Here, $\lambda = \pm 1$ is the CP of the final state, ϕ_1 is a parameter that describes the CP violation, and $\Delta\mathrm{m} = (3.3365 \pm 0.0125) \times 10^{-10}\,\mathrm{MeV}/c^2$ [1]. Using $K_L^0 \approx K_2^0$, $J^{PC} = 1^{--}$

doi:10.6342/NTU202500482

for ϕ and J=0 for B^0 (or $\overline{B}^0$), we get $\lambda = (+1) \times (-1) \times (-1)^{L=1} = +1$. Hence, the decay mode $B^0 \to \phi K_L^0$ can provide a measurement of $\sin 2\phi_1$.

doi:10.6342/NTU202500482

doi:10.6342/NTU202500482

Chapter 2

Belle II experiments

Starting data taking from the end of 2019, the Belle II experiment is an international collaborative experiment that aims to explore the fundamental nature of elementary particles. Upgraded from the detectors of Belle experiment (from 1999 to 2009), new data acquisition system of Belle II detectors will meet the requirement of noticeably higher reaction rates.

In this chapter, a brief introduction of several Belle II constituent detectors will be presented [5].

2.1 SuperKEKB accelerator

Inheriting the previous KEKB accelerator at Belle , the SuperKEKB is a circular e^+e^- collider of circumference about 3km. The configuration of particle beams (7 GeV and 4 GeV for electron and positron, respectively) results in a center-of-mass energy $\sqrt{s}$ about 10.58 GeV , slightly above the bottom threshold to produce an $\Upsilon(4S)$ resonance subsequently decaying to a pair of B mesons. With this asymmetric energy scheme, these two

doi:10.6342/NTU202500482

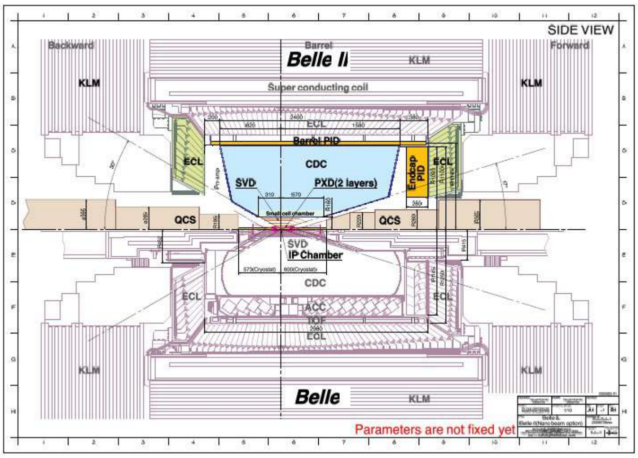

Figure 2.1: Upgraded Belle II detectors.

B mesons will possess net momenta in the lab frame, making their decay products easier to detect.

While the Large Hadron Collider (LHC) of the European Organization for Nuclear Research (CERN) possesses the highest center-of-mass energy (of order TeV) among all the other accelerators, SuperKEKB has achieved a remarkable world record of instantaneous luminosity at the end of 2024 ($5.1 \times 10^{34}\,\mathrm{cm}^{-2}\mathrm{s}^{-1}$). The schematic view of the SuperKEKB is illustrated in Figure 2.2.

doi:10.6342/NTU202500482

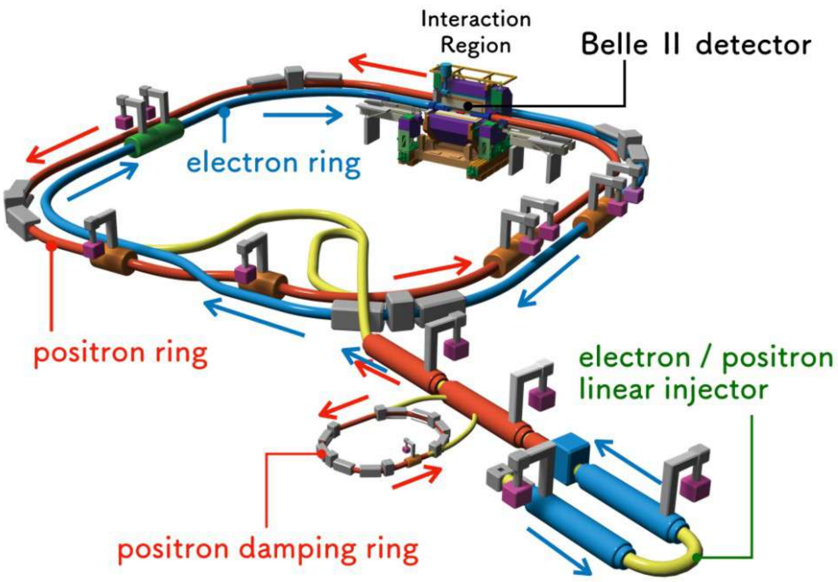

Figure 2.2: SuperKEKB accelerator configuration

2.2 Pixel Detector (PXD)

Aimed for precision vertex reconstruction of B-meson decay, PXD is a silicon pixel detector located close to the beam pipe. Due to the anticipated large beam-related background rate, PXD adopts a new concept of double-layer (r = 14 mm and 22 mm) DEPFET (DEPleted Field Effect Transistor) pixel sensors. By the combination of detection and internal amplification, these sensors can be made very flimsy and can provide high signal-to-noise ratios.

Due to proximity to the interaction point (IR), the PXD data needs to be filtered using information from the outer tracking detectors to prevent the data volume becoming unmanageable.

doi:10.6342/NTU202500482

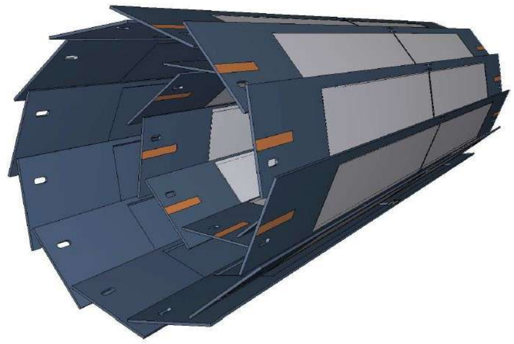

Figure 2.3: Schematic view of the geometrical arrangement of the sensors for the PXD.

2.3 Silicon Vertex Detector (SVD)

SVD comprises four layers of double-sided silicon strip detectors (DSSDs) and covers the full Belle II angular acceptance(17° to 150°). Together with CDC and PXD, SVD can measure the two B decay vertices. It is also capable of reconstructing K-short mesons that decay to pair of charged pions outside the PXD.

2.4 Central Drift Chamber (CDC)

CDC is a large cylindrical detector (radii 160mm and 1130mm for the inner and outer cylinders, respectively) with a polar angle acceptance from 17° to 150°. It is filled by a $He - C_2H_6$ mixture of gas.

In a strong magnetic field of about 1.5 Tesla, CDC can reconstruct charged tracks and make a precise measurement of their momenta. Utilizing different distribution behaviors of ionization energy loss (dE/dx) , CDC is able to provide PID information for charged

doi:10.6342/NTU202500482

final-state particles(e.g. π, K, p, e, μ).

2.5 Particle Identification (PID systems)

Two new charged particle identification devices are mounted in the barrel and endcap regions. These are the Time of Propagation (TOP) detector and Aerogel Ring-Imaging Cherenkov (ARICH) detector. With even faster electronics read-out and higher performance, they can provide well-improved K/π discrimination.

2.5.1 Time of Propagation (TOP)

TOP covers a range of polar angle between 32° to 120° in the barrel region. The angles at which Cherenkov photons are emitted vary depending on the mass of different particles with the same momentum. The difference in emitting angles leads to different optical lengths and propagation time of the photons. With total internal reflection , the emitted photons can be collected by the photomultiplier tubes.

2.5.2 Aerogel Ring-Imaging Cherenkov detector (ARICH)

ARICH takes charge of particle identification in the forward end-cape. It utilizes two layers of aerogel radiator as the medium with different indices of refraction. The Cherenkov photons form a cone of light around the particle's trajectory, which is subsequently captured as a ring of characteristic radius depending on the Cherenkov angle.

doi:10.6342/NTU202500482

2.6 Electromagnetic Calorimeter (ECL)

ECL is an electromagnetic calorimeter composed of about 8000 Caesium Iodide CsI(Tl)(Thallium-doped) scintillation crystals in total , with a coverage between polar angle 12.4 to 155.1°.These crystals distributed in three main regions of ECL (barrel, forward endcap and backward endcap).

High energy electrons (or positrons) will emit Bremsstrahlung photons when interacting with atomic nuclei they traversed, and each energetic photon will subsequently give rise to a pair-produced electron-positron, leading to an electromagnetic (EM) shower in ECL. A high energy photon arising from collision events will possibly end up with an EM shower as well. ECL chooses CsI(Tl) as the scintillation crystals (with a short radiation length $X_0 \cong 1.9$ cm) to restrict the electromagnetic showers within a compact region. The chief duty of ECL is to measure the energy deposited to the crystals from energetic electrons, positrons and photons , with an expected energy resolution σ E / E = 0.2 % / $\sqrt{E(GeV)}$.

2.7 K$_L$ and Moun detector (KLM)

Located outside the superconducting solenoid, alternate layers of iron plates and detector elements constitute the main part of KLM. Muons with momenta beyond 600 MeV are able to be identified in KLM. K_L^0's interacting with the iron plates in KLM will give rise to a hadronic showers that can be detected and reconstructed.

doi:10.6342/NTU202500482

Chapter 3

Event Selections

3.1 Monde-Carlo Samples

All simulated samples (referred to as Monte-Carlo or MC) in this study are processed using Belle2 Analysis Software Framework (`basf2`), version `light-2305-korat`.

3.1.1 Signal Samples

To study adequate event selections, we generate 1 million run-independent Monte-Carlo simulated events $B^0 \to \phi(\to K^+K^-) K_L^0$ (with B-mixing) using the `EvtGen` package [6](These samples are called **signal MC**). In each event, one of the neutral B mesons decays through the desired channel, while the partner non-signal B meson decays generically according to the branching fraction listed in the Belle II decay table.

3.1.2 Background Samples

Generic background MC samples can be classified into two main categories :

doi:10.6342/NTU202500482

$*$ $e^+e^- \to \Upsilon(4S) \to B^+B^-$ or $B^0\overline{B}^0$ events. These processes are called **BB background** in the Belle II jargon. Both of the B mesons undergo a generic decay following the branching fractions listed in the Belle II decay table. We use the generated level information [7] to discard signal events in these processes.

$*$ $e^+e^- \to q\overline{q}$ events (q denotes u, d, c, or s quark) . In the realm of B physics, these processes are referred to as **qq background** or **continuum background**. Due to a large amount, this dominant type of background will be tackled using the technique called **Continuum Suppression**, which will be detailed in chapter 3.

We use 200 fb^{-1} officially-produced `MC15ri (BGx1)` qq background samples for Continuum Suppression. And then we process 699.235 fb^{-1} official `MC15rd` background samples (including BB and qq background) for the following fitting procedure.

3.2 Reconstruction and Selections

3.2.1 Reconstruction of ϕ

For the reconstruction of charged kaons(K^+ & K^-), we use the standard "good" type of kaon lists , with the following selections :

$*$ dr < 0.5 cm & | dz | < 2 cm , where dr is the transverse distance between the point of closest approach (POCA) and the z-axis , and dz is the z coordinate of the POCA (with IP at origin)

$*$ polar angle θ of the tracks be within CDC acceptance and the number of CDC hits be greater than 20

doi:10.6342/NTU202500482

∗ global Kaon-ID > 0.5

ϕ meson is an $s\bar{s}$ resonance of mass 1.019 GeV with a narrow width about 0.0042 GeV. We put a relatively loose cut on the invariant mass of the ϕ candidates: 0.99 < M <1.05 GeV and use this variable (called M_ϕ or phi_M in the rest of the thesis) as one of the fitting variables.

3.2.2 Reconstruction of K_L^0

K_L^0 candidates are all reconstructed from ECL clusters. To discriminate the true K_L^0 from a tremendous amount of fake K_L^0, we apply a trained MVA classifier which was trained and validated by Jheng-Hou.Su [8]. It was based on some information from the ECL clusters to distinguish K_L^0 from other neutral clusters (e.g. $\bar{n}$ or γ). The classifier will give an MVA score (range from zero to one) to the reconstructed ECL clusters. We choose ECL clusters with MVA > 0.5 to be candidates K_L^0.

3.2.3 Reconstruction of B^0

Considering the inaccuracy of the momenta of K_L^0 candidates reconstructed from ECL clusters, we use a module `modularAnalysis.reconstructDecayWithNeutralHadron` in `basf2` to reconstruct candidate B^0. Two constraints are assumed :

∗ IP constraint : Assume the direction of the momentum of a K_L^0 candidate is from the interaction point(IP) to that ECL cluster.

∗ B mass constraint : Assume this candidate was decayed from a B^0 or $\overline{B}^0$. Using four-momentuem conservation (with the mass of B^0 , K_L^0 and ϕ given) , we can calculate

doi:10.6342/NTU202500482

the magnitude of a K_L^0 momentum. Once the momentum of a candidate K_L^0 is obtained, it is combined with a candidate ϕ to reconstruct a candidate B^0.

The center-of-mass(CMS) energy $\sqrt{s}$ of the SuperKEKB accelerator in an on-resonance run is about 10.58 GeV to produce an $\Upsilon(4S)$ resonance subsequently decays to a pair of B mesons. In the CMS frame, these two B will share half of the energy. Accordingly, the center-of-mass momentum of a neutral B candidate (we call it P_B^* or pB_star in the thesis) will have a peak value at about 0.33 GeV if there is a signal event. We put a selection $P_B^* < 1$ on the reconstructed B^0 candidates and use it as a fitting variable.

The helicity angle θ_2, defined in the rest frame of ϕ (ref. Figure 3.1) [9], can serve as another fitting variable to separate signal events from background. The spin-1 vector meson ϕ decays to a pair of spin-0 pseudo-scalar mesons K^+K^-, resulting in an angular distribution proportional to $|d^1_{0,0}|^2 = \cos\theta_2^2$. Consequently, the cosine value of θ_2 will have a peak at ± 1 , provided there is a genuine ϕ that decays to K^+K^-. We call it $\cos\theta_K$ or cosTheta_K in the rest of this thesis.

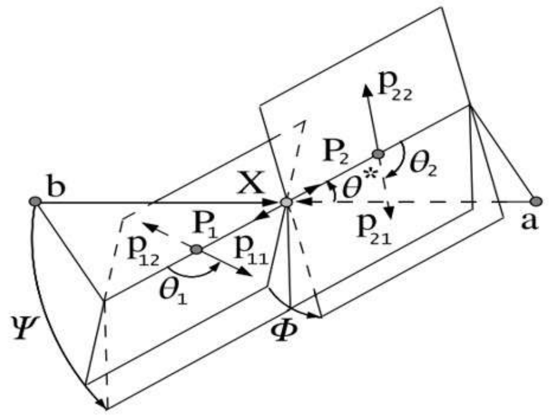

Figure 3.1: Definition of the helicity angle viewed in the rest frame of ϕ meson. Where X , P_2 and P_{21} are B^0 , ϕ and K^+ meson, respectively.

doi:10.6342/NTU202500482

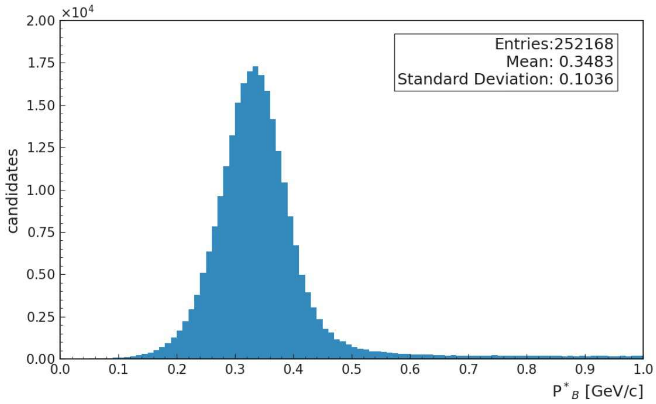

(a) P_B^*

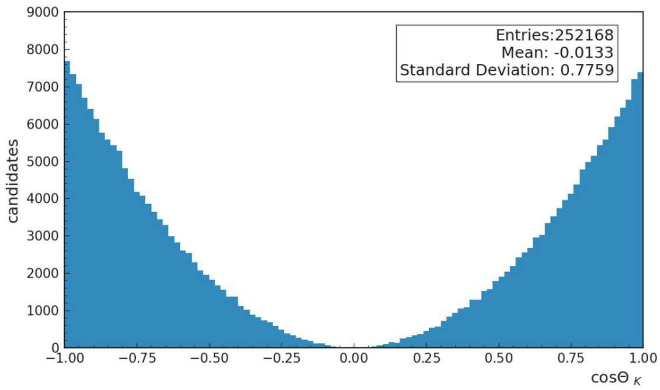

(b) $\cos\theta_K$

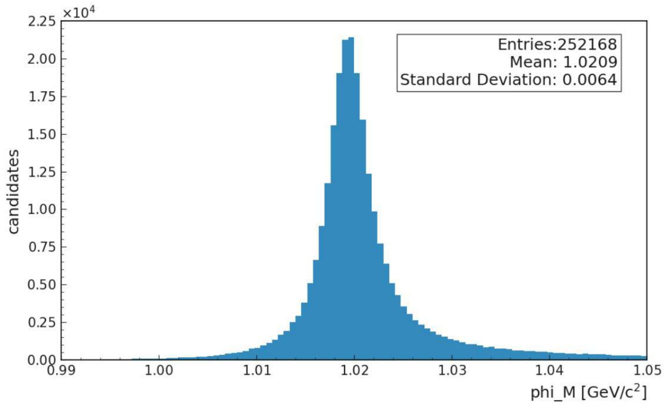

(c) M_ϕ

Figure 3.2: Fitting variable distribution of signal MC

doi:10.6342/NTU202500482

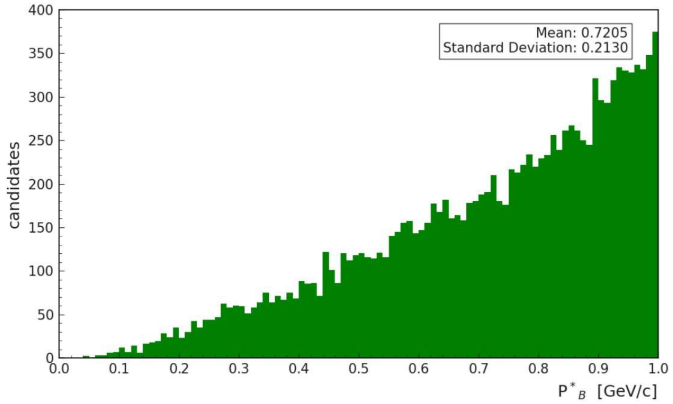

(a) P_B^*

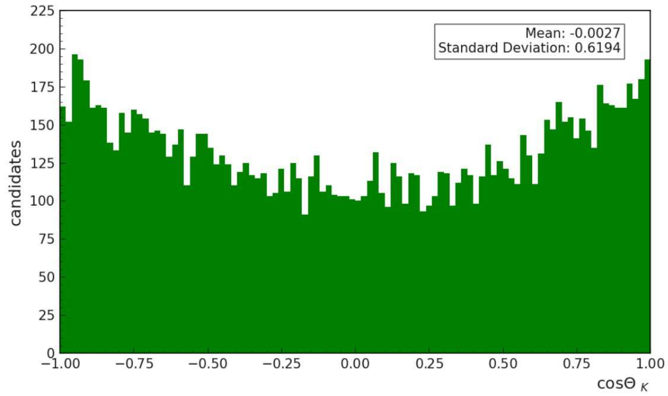

(b) $\cos\theta_K$

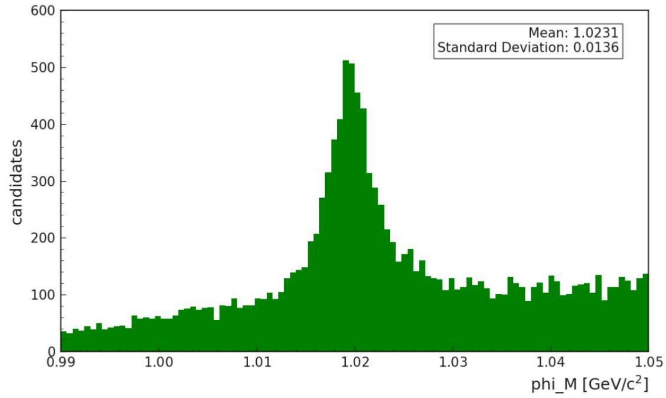

(c) M_ϕ

Figure 3.3: Fitting variable distribution of BB background

doi:10.6342/NTU202500482

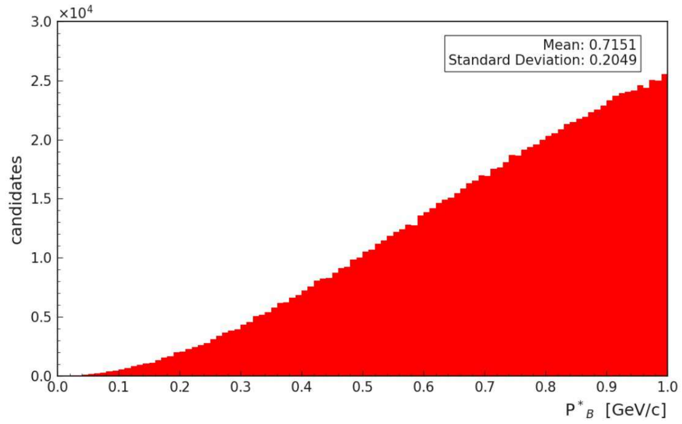

(a) P_B^*

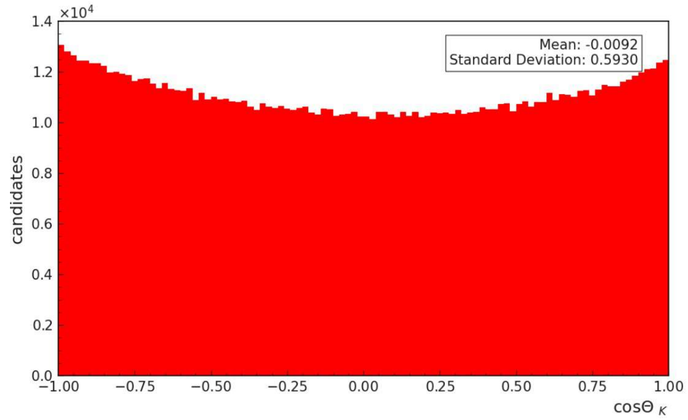

(b) $\cos\theta_K$

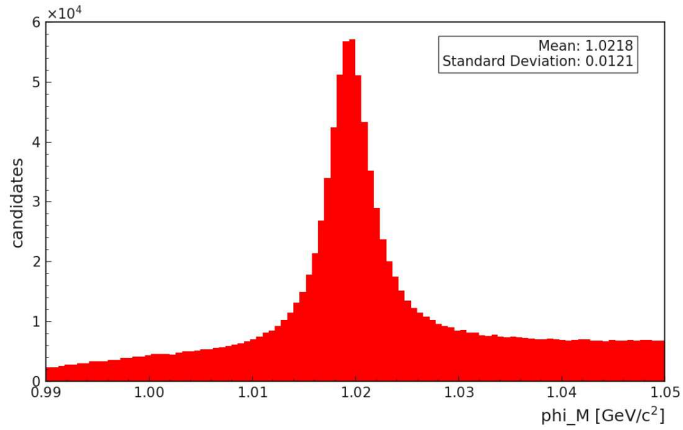

(c) M_ϕ

Figure 3.4: Fitting variable distribution of qq background

doi:10.6342/NTU202500482

doi:10.6342/NTU202500482

Chapter 4

Continuum Suppression

Studies for B decays suffer a dominant background type arising from non-resonant $e^+e^- \rightarrow q\bar{q}$ hadronic events (where $q = u, d, c$ or s) , which are referred to as **continuum background** or **qq background**. This type of process will typically give rise to several tracks per event, and thus there is a great opportunity to randomly reconstruct a tremendous amount of B^0 candidates that pass the event selection outlined in the previous chapter.

Fast Boosted Decision Tree (`FastBDT`) is the default multivariate algorithm in `basf2` to deal with continuum background suppression. Continuum Suppression exploits the distinct difference in the overall ”event shape” between a BB event (to which our signal belongs) and a qq event. Some of this kind of event shape information is used to train a classifier that determines whether a B^0 candidate resembles a signal B meson or a misreconstructed background.

In a BB event, the two B mesons are nearly stationary due to the mass of $\Upsilon(4S)$ being only slightly above the bottom threshold. Consequently, their decay products are uniformly distributed in the center-of-mass frame. On the other hand, light quarks produced

doi:10.6342/NTU202500482

in a qq event inherit large initial momenta, which, after fragmentation into hadrons, will produce a highly collimated jet-like distribution, as illustrated in Figure 4.1.

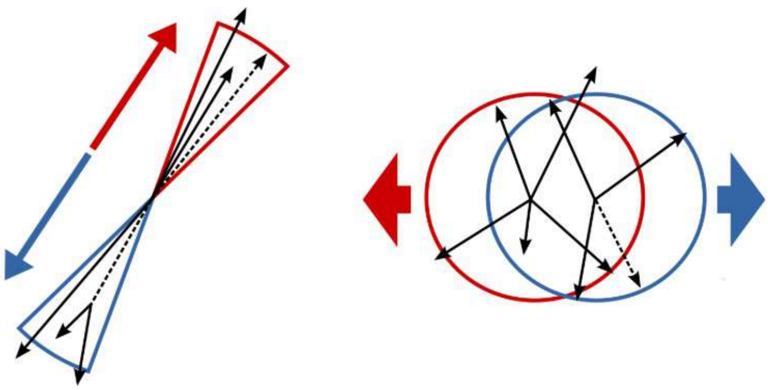

Figure 4.1: Distribution (shape) of particles in a qq event (left) and a BB event (right)

4.1 Training Variables

We used 32,740 signal MC candidates and 100 fb^{-1} `MC15ri` qq background (31,650 entries) to train the FastBDT classifier. The list of training variables follows:

∗ abs(cosθ_B) – θ_B is the angle between the momentum of a B^0 candidate and the z-axis in the center-of-mass frame

∗ R2 – ratio of the 2nd and zeroth Fox-Wolfram moments

∗ ThrustOm – magnitude of the thrust vector of the rest of event of a B^0 candidate

∗ cosTBTO – cosine value of the angle between the thrust axis of a B^0 candidate decay products and that of the rest of event

doi:10.6342/NTU202500482

∗ cosTBz – cosine value of the angle between the thrust axis of a B^0 candidate decay products and the z-axis

∗ KSFW moments– some kinds of Fisher discriminants developed by the Belle collaboration

∗CleoCones – some multivariate discriminant variables introduced by the CLEO collaboration in the context of charmless B decays (b to u,d or s)

To improve the separation power of the classifier in signal region, defined as $0.15 < P_B^* < 0.55$ GeV, we choose qq training samples in this region.

For the evaluation of training performance, we use 500,000 signalMC events along with $100 fb^{-1}$ `MC15ri` qq background for the testing procedure. The result is illustrated in Figure 4.2.

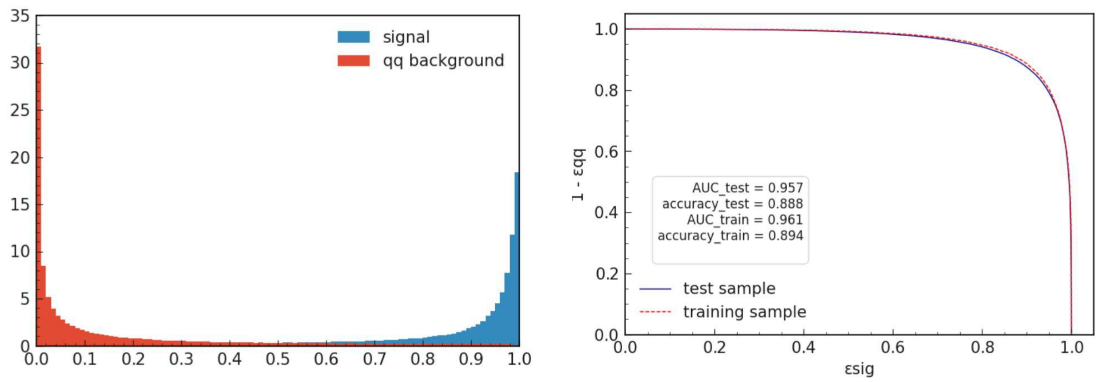

(a) BDT output (b) ROC curves

Figure 4.2: The training result. In Figure 4.2(a), histograms are normalized. In Figure 4.2(b), AUC stands for area under curve.

doi:10.6342/NTU202500482

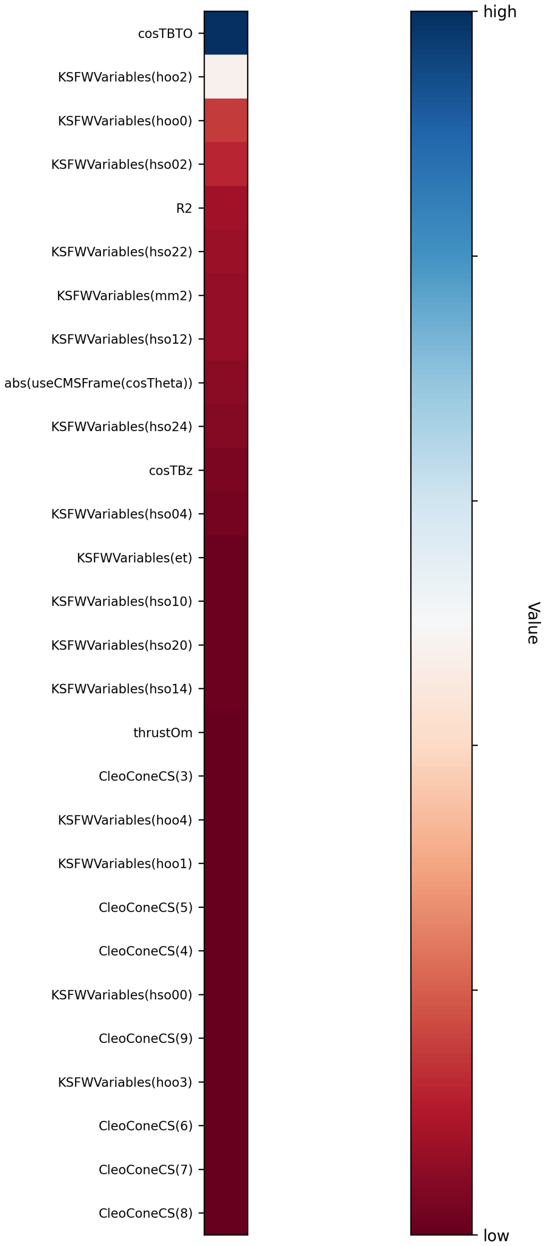

Figure 4.3: Importance for each training variable

doi:10.6342/NTU202500482

The decision on cut values of the BDT output is based on signal to background significance after the corresponding cut. A commonly-used evaluation is the Figure of Merit (F.O.M.) , defined as

$$F.O.M. \equiv \frac{Nsig}{\sqrt{Nsig + Nbkg}} \tag{4.1}$$

Here, Nsig and Nbkg denotes the number of signal and background events (BB plus qq) left, respectively, within the signal box. The signal box is defined by the conditions : $0.15 < P_B^* < 0.55$ GeV & $1.00 < M_\phi < 1.04$ GeV. Figure 4.4a shows the corresponding retention for various cut values. The FOM curve is depicted in Figure 4.4b, where we scale the integrated luminosity to that of data. We calculate the error bars using propagation of uncertainty. According to the curve, a cut BDT > 0.93 is adopted to avoid large errors in FOM values.

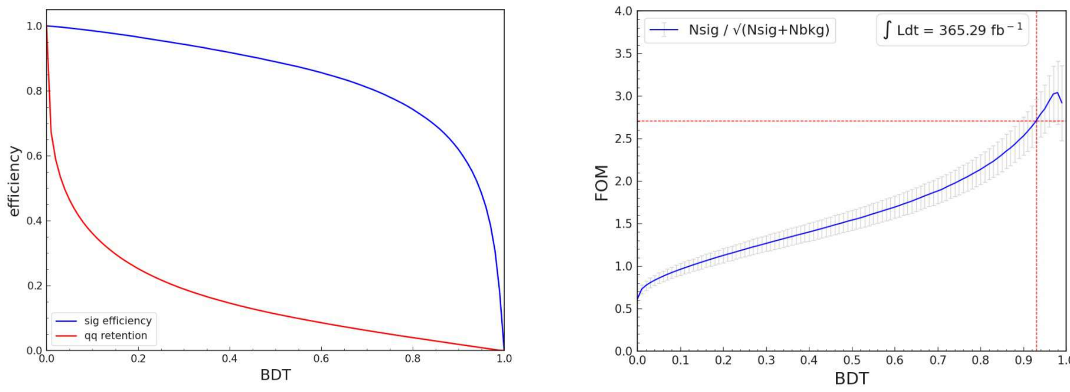

(a) Retention after BDT cut

(b) FOM curve

Figure 4.4

doi:10.6342/NTU202500482

4.2 Best Candidate Selection

After the cut on Continuum Suppression BDT output, multiple candidates are still present in each event. Table 4.1 lists the multiplicities for each type of samples. We select a B^0 candidate with the largest MVA value of K_L^0 as the best candidate in each event. Table 4.2 is the summary of the final selections. Distributions of the three fitting variables after the final selections are depicted in Figures 4.5, 4.6 and 4.7. The efficiency table for consecutive selections is summarized in Table 4.3. Table 4.4 list the corresponding candidates/ events left for BB and qq background after each selection.

sample	multiplicity
signal MC	1.005
BB	1.005
qq	1.004

Table 4.1: Multiplicities for each type of sample

doi:10.6342/NTU202500482

$K^{\pm}$	Kaon ID > 0.5	ϕ	$0.99 < M < 1.05$ GeV
	polar angle in the CDC acceptance	K_L^0	MVA > 0.5
	number of CDC hits > 20		
	$dr < 0.5$ cm	B^0	$P_B^* < 1$ GeV
	$\lvert dz \rvert < 2$ cm		BDT > 0.93
			max K_L^0 MVA

Table 4.2: Summary of the final selections

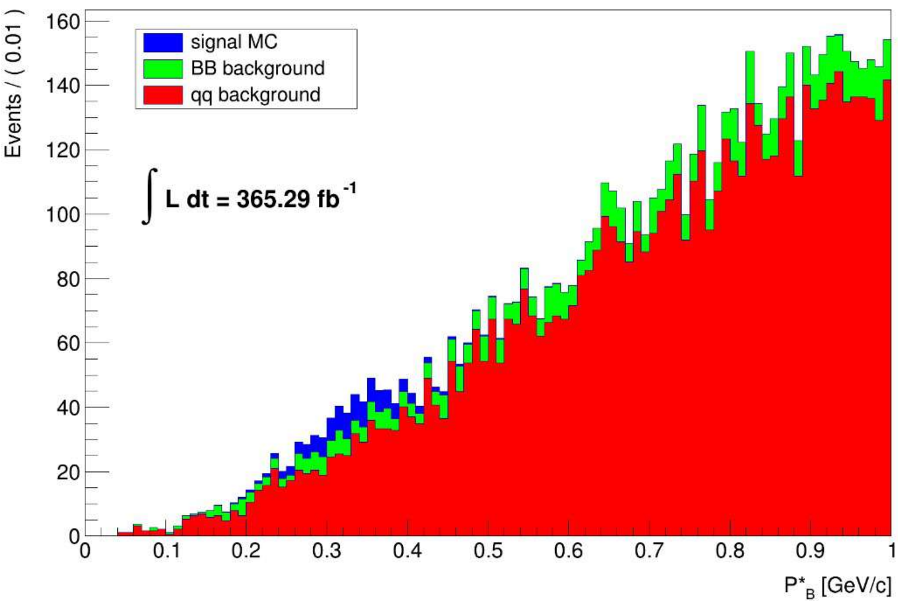

Figure 4.5: Distribution of P_B^* after all the event selections

doi:10.6342/NTU202500482

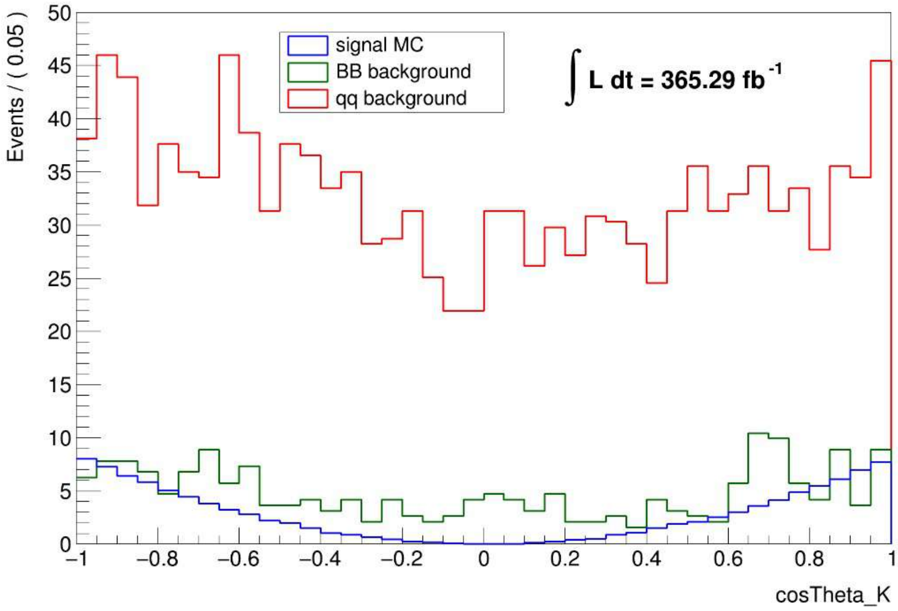

Figure 4.6: Distribution of $\cos\theta_K$ after all the event selections

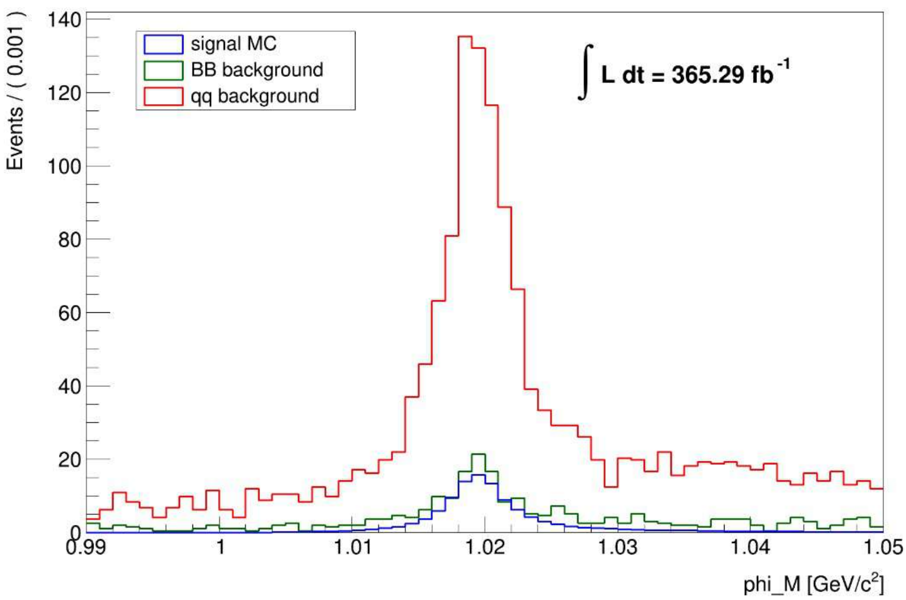

Figure 4.7: Distribution of M_ϕ after all the event selections

doi:10.6342/NTU202500482

cut	efficiency
$1.00 < M_\phi < 1.04$ GeV & K_L^0 MVA > 0.5	44.1%
$P_B^* < 1$ GeV	25.2%
BDT > 0.93	13.9%
Best Candidate	13.8%

Table 4.3: Efficiency table for consecutive selections

cut	BB	qq
pre-selection	13189	1104830
BDT > 0.93	1522	14003
Best Candidate	1515	13954

Table 4.4: Candidates/events left after consecutive selections. The luminosity for BB and qq background is $699.235 fb^{-1}$

doi:10.6342/NTU202500482

doi:10.6342/NTU202500482

Chapter 5

Signal Extraction

5.1 Fitting Strategy

A three-dimensional unbinned maximum likelihood fit is planned to extract signal events from background noise. Since the shape of the three fitting variables (P_B^*, $\cos\theta_K$ and M_ϕ) are same for BB and qq background, we model them together. Before the PDF modeling, we have to check the correlation between three fitting variables for signal MC and BB+qq background. Tables 5.1 and 5.2 show the correlation matrices for these variables. Figures 5.1, 5.2, 5.3, 5.4, 5.5, and 5.6 are the scatter plots for them.

signal MC	P_B^*	$\cos\theta_K$	M_ϕ
P_B^*	—	-0.076%	$4.4 * e^{-5}$
$\cos\theta_K$	-0.076%	—	-0.355%
M_ϕ	$4.4 * e^{-5}$	-0.355%	—

Table 5.1: Correlation matrix for signal MC

doi:10.6342/NTU202500482

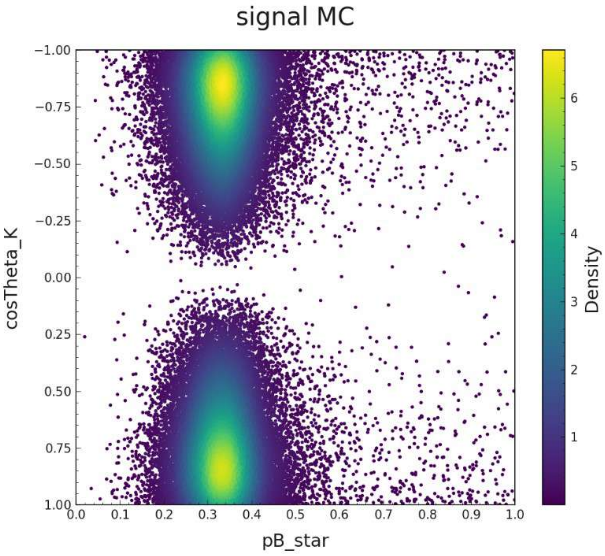

Figure 5.1: Scatter plot of P_B^* v.s. $\cos\theta_K$ for signal MC

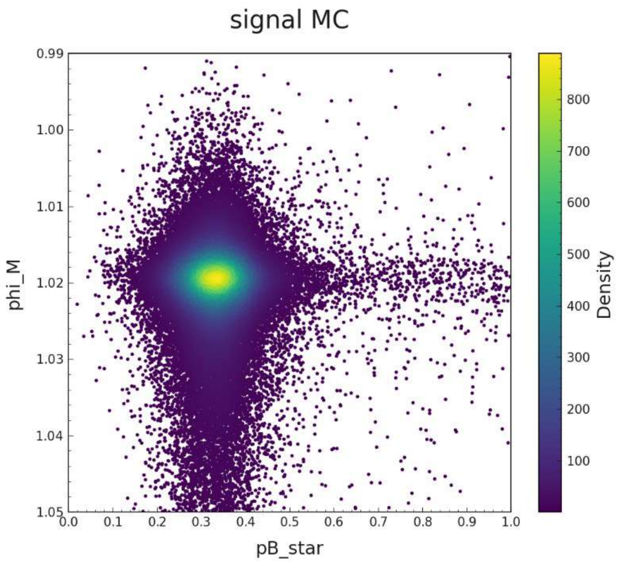

Figure 5.2: Scatter plot of P_B^* v.s. M_ϕ for signal MC

doi:10.6342/NTU202500482

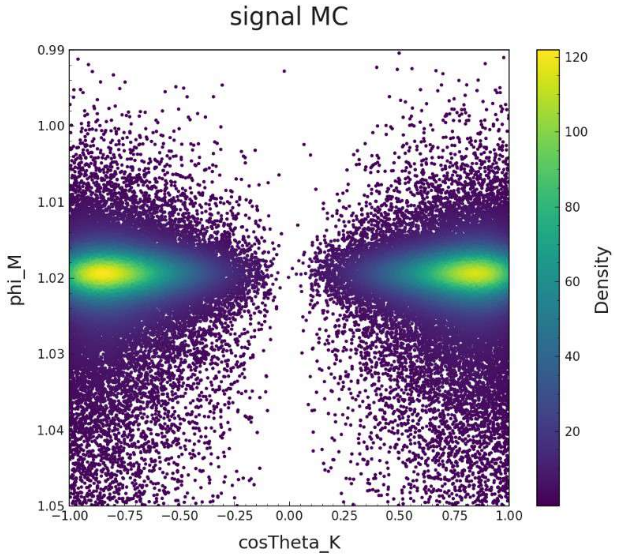

Figure 5.3: Scatter plot of $\cos\theta_K$ v.s. M_ϕ for signal MC

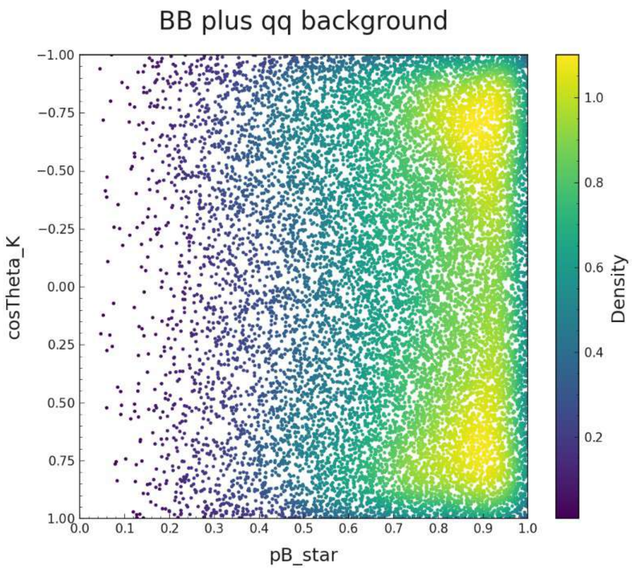

Figure 5.4: Scatter plot of P_B^* v.s. $\cos\theta_K$ for background

doi:10.6342/NTU202500482

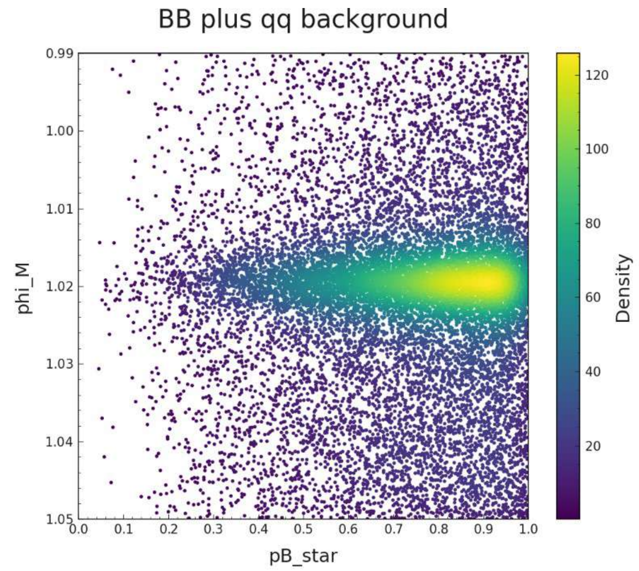

Figure 5.5: Scatter plot of P_B^* v.s. M_ϕ for background

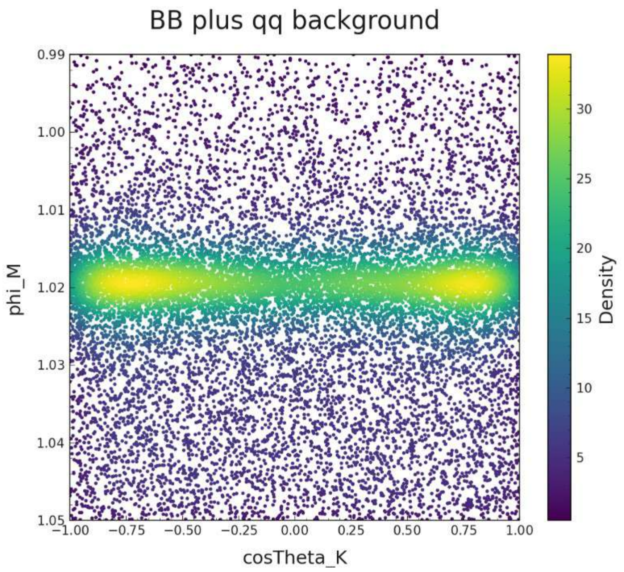

Figure 5.6: Scatter plot of $\cos\theta_K$ v.s. M_ϕ for background

doi:10.6342/NTU202500482

BB plus **qq**	P_B^*	$\cos\theta_K$	M_ϕ
P_B^*	—	0.888%	-0.032%
$\cos\theta_K$	0.888%	—	0.394%
M_ϕ	-0.032%	0.394%	—

Table 5.2: Correlation matrix for background

5.2 PDF Modeling

To precisely describe the shape of M_ϕ in a signal event, we combine signal MC with $200 fb^{-1}$ BB & $100\ fb^{-1}$ qq background (run-independent). The dimension M_ϕ in a signal event is parametrized by the resulting mean and width of the Breit-Wigner shape.

Table 5.3 summarizes the shapes of all PDFs. Figures 5.7, 5.8, 5.9, 5.10, 5.11 and 5.12 are the results of the modeling.

sample	P_B^*	$\cos\theta_K$	M_ϕ
signal MC	Gaussian + Voigtian (signal region)	$2bx^2+ax+(1-b)$	Breit-Wigner + 1st-order polynomial
background (**BB** plus **qq**)	$1-\text{sech}(cx)$	$2ex^2+(1-e)$	Breit-Wigner + 1st-order polynomial

Table 5.3: Shapes of all PDFs

doi:10.6342/NTU202500482

5.3 Extended Maximum Likelihood Fit

Signal events are extracted using the extended maximum likelihood estimator. From the similarity in the shapes of M_ϕ between signal MC and background, we infer that a significant number of genuine ϕ's are present in the background. Consequently, we split the background term in the total fit model into two components: the peaking term and the non-peaking term. The peaking term is described by a Breit-Wigner distribution, with its mean and width fixed to those of the signal, while the non-peaking term is modeled using a linear polynomial.

The likelihood for each event is described by

$$L_i = N_{sig} \times P_{sig} + N_{bkg\_peaking} \times P_{bkg\_peaking} + N_{bkg\_non\_peaking} \times P_{bkg\_non\_peaking}, \tag{5.1}$$

where the three PDFs are

$$\begin{aligned} P_{sig} =& [\text{gfrac} \times Gauss(P_B^*; \mu, \sigma) + (1 - \text{gfrac}) \times Voigt(P_B^*; \text{mean , width , sigma})] \\ & \times \text{2nd-order polynomial}(\cos\theta_K; a, b) \\ & \times \textit{Breit-Wigner}(\text{M}_\phi; \text{mean, width}) \end{aligned} \tag{5.2}$$

$$\begin{aligned} P_{bkg\_peaking} =& [1 - sech(P_B^*; c)] \times \text{2nd-order polynomial}(\cos\theta_K; e) \\ & \times \textit{Breit-Wigner}(\text{M}_\phi; \text{mean, width}) \end{aligned} \tag{5.3}$$

$$\begin{aligned} P_{bkg\_non\_peaking} =& [1 - sech(P_B^*; c)] \times \text{2nd-order polynomial}(\cos\theta_K; e) \\ & \times \text{1st-order polynomial}(\text{M}_\phi; f). \end{aligned} \tag{5.4}$$

doi:10.6342/NTU202500482

The best solution is to maximize

$$L = \frac{exp[-(N_{sig} + N_{bkg\_peaking} + N_{bkg\_non\_peaking})]}{N!} \times \prod_{i=1}^{N} L_i. \tag{5.5}$$

Here, N_{sig}, $N_{bkg\_peaking}$ and $N_{bkg\_non\_peaking}$ denotes the number of signal events, peaking background events, and background events without peaks (in the variable M_ϕ), respectively.

The fitting samples consist of signal MC, BB background and qq background. We give a weight to each event in signal MC, which is equal to the expected signal yields under luminosity 365.29 fb^{-1}divided by the number of signal MC events. The event number of BB and qq background is scaled to identical luminosity using a background weight factor (number of events under 365.29 fb^{-1}/number of events under 699.235 fb^{-1}). Figures 5.13 , 5.14 and 5.15 depict the fitting results, where we project the total fit model and the three constituent PDFs onto each fitting dimension.

5.4 Fitter Test

We perform a Gsim ensemble test to validate the robustness of the fitter. The number of pseudo-experiments is set to 1,000. In each experiment, k events are drawn from signal MC, where k obeys a Poisson distribution with mean value corresponding to the expected signal yields under 365.29 fb^{-1}. Similarly , we randomly select events from BB and qq background, separately, where the two numbers of drawn events obey the Poisson distribution with mean values being the counting numbers scaled to the same luminosity. We

doi:10.6342/NTU202500482

fit the overall PDF to the combined dataset and calculate the pull value.

The resulting distribution is plotted in Figure 5.16.

According to the pull distribution after fitter test, there is a bias in the fitter. However, the result is consistent with that obtained after a single fit.

To find out which background sample contributes to the extra signal yields, we perform two fits using the identical total fit model. The first fitting sample consists of signal MC combined with BB background, while the second one includes signal MC and qq background. From figures 5.17 and 5.18 we conclude that BB background is the origin of the bias. Tables 5.4 and 5.5 summarize the top three charged and mixed decay modes for BB background, as obtained from the generator-level information [7]. All events in the tables are selected in the signal region: $0.15 < P_B^* < 0.55$ GeV.

BplusMode	events	BminusMode	events
$B^+ \to \phi K^{*+}$	19	$B^- \to \phi K^{*-}$	27
$B^+ \to \rho^+ \overline{D}^0$	5	$B^- \to \rho^- D^0$	16
$B^+ \to \overline{D}^0 \mu^+ \nu_\mu$	5	$B^- \to D^{*0} \mu^- \overline{\nu}_\mu$	8

Table 5.4: Charged decay modes for BB background in the signal region after all the event selections. The luminosity is 699.235 fb^{-1}.

doi:10.6342/NTU202500482

`B0Mode`	events	`Bbar0Mode`	events
$B^0 \to \phi K^{*0}$	14	$\overline{B}^0 \to \phi \overline{K}^{*0}$	16
$B^0 \to \phi K_S^0$	12	$\overline{B}^0 \to \rho^- D^+$	13
$B^0 \to \rho^+ D^-$	11	$\overline{B}^0 \to \phi K_S^0$	12

Table 5.5: Mixed decay modes for BB background in the signal region after all the event selections. The luminosity is 699.235 fb^{-1}.

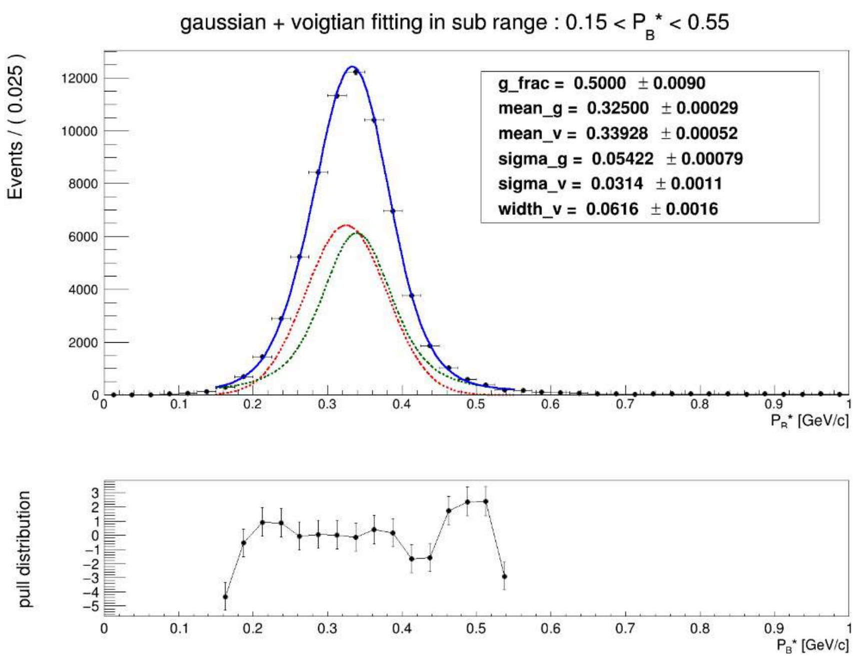

Figure 5.7: Shape of P_B^* of signal MC

doi:10.6342/NTU202500482

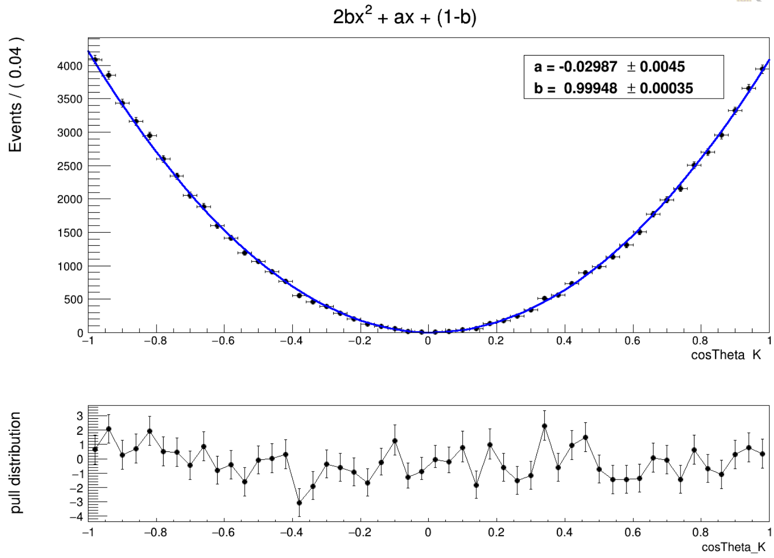

Figure 5.8: Shape of $\cos\theta_K$ of signal MC

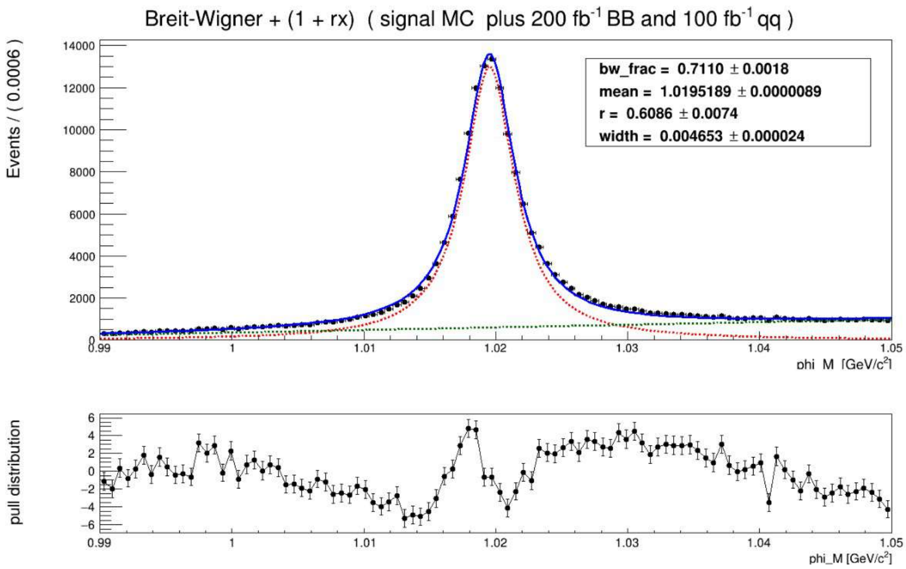

Figure 5.9: Shape of M_ϕ of signal MC plus background

doi:10.6342/NTU202500482

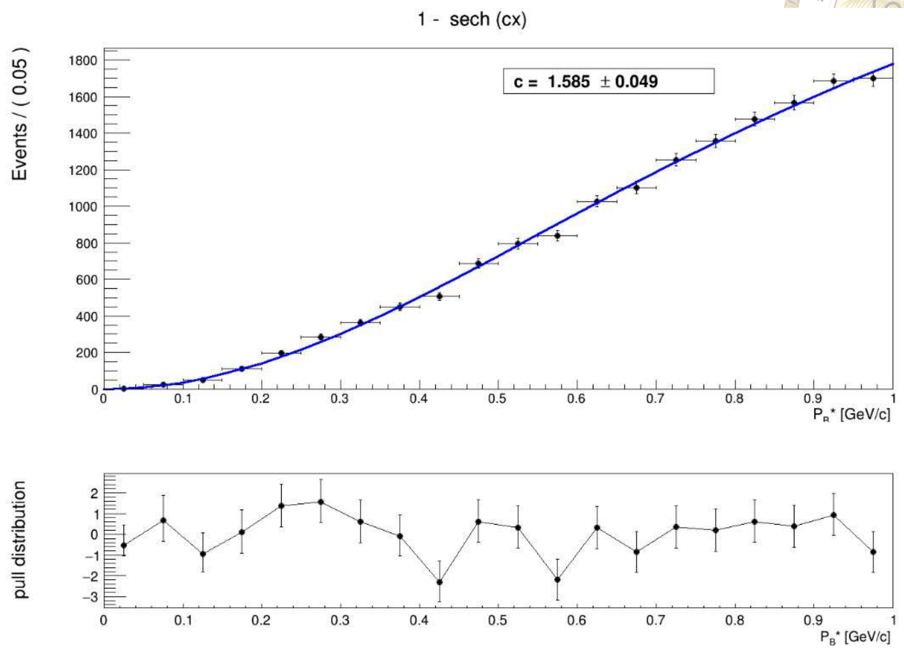

Figure 5.10: Shape of P_B^* of background

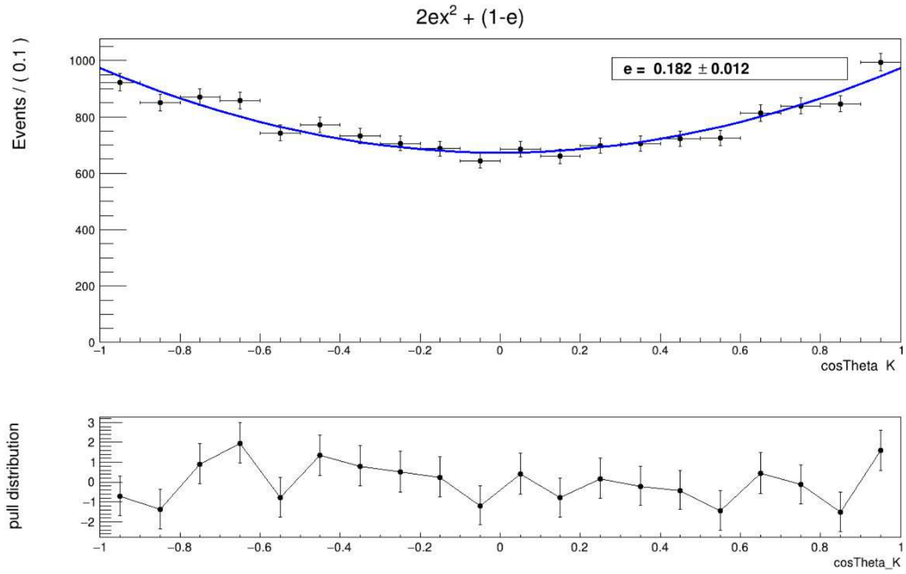

Figure 5.11: Shape of $\cos\theta_K$ of background

doi:10.6342/NTU202500482

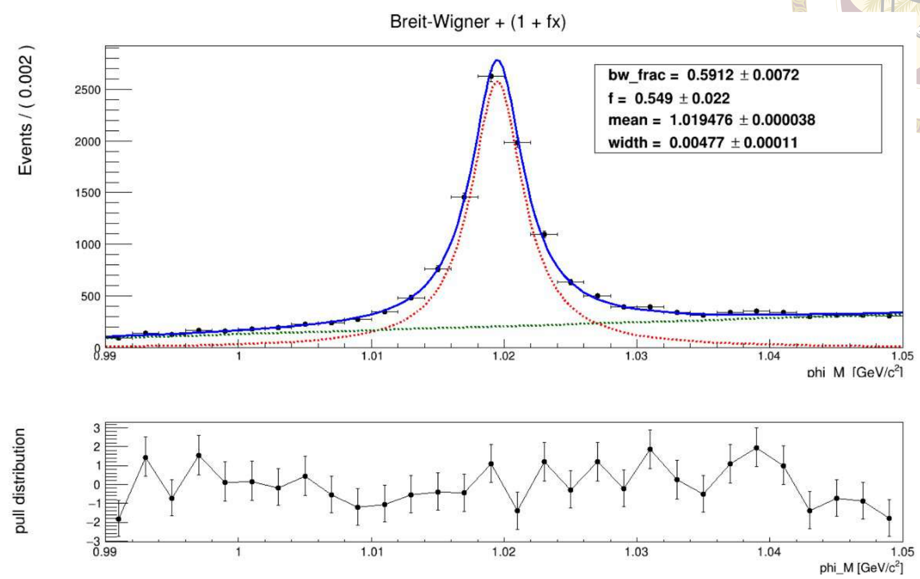

Figure 5.12: Shape of M_ϕ of background

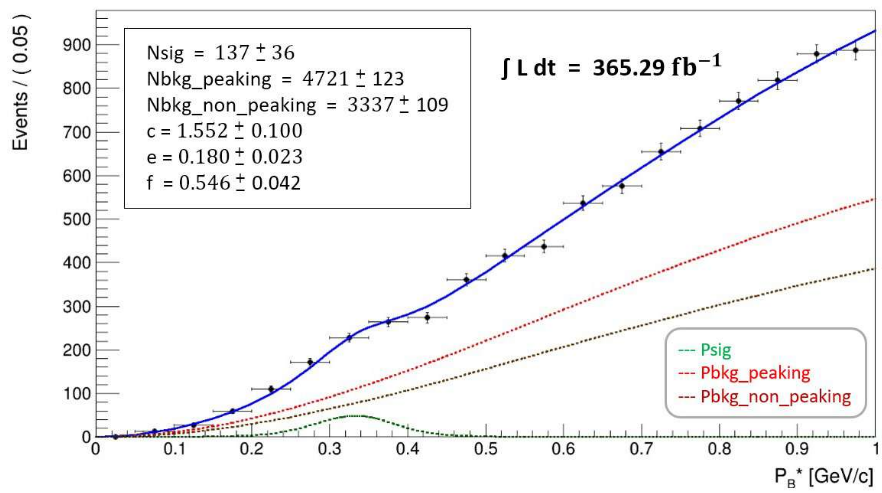

Figure 5.13: Projection of the fitting result onto P_B^* dimension

doi:10.6342/NTU202500482

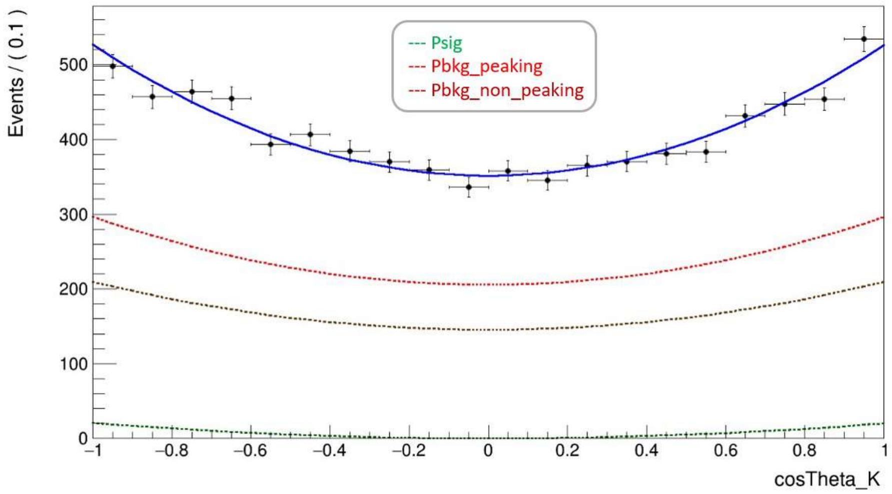

Figure 5.14: Projection of the fitting result onto cosθ_K dimension

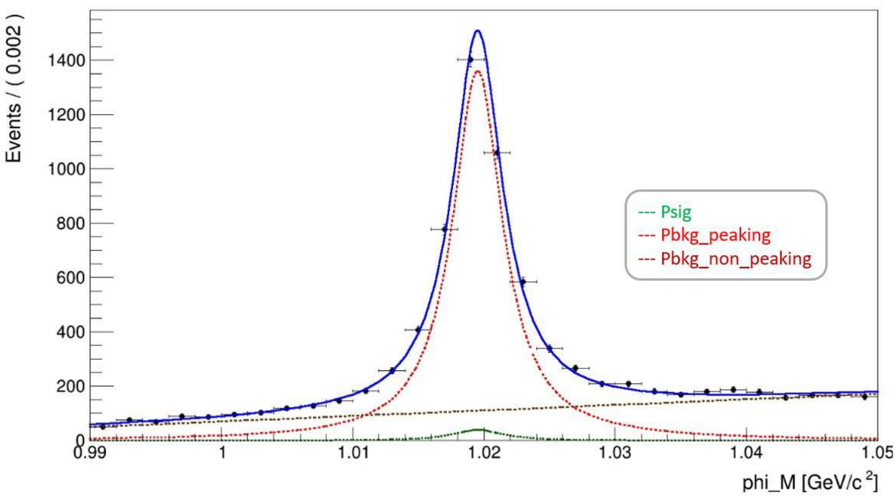

Figure 5.15: Projection of the fitting result onto M$_\phi$ dimension

doi:10.6342/NTU202500482

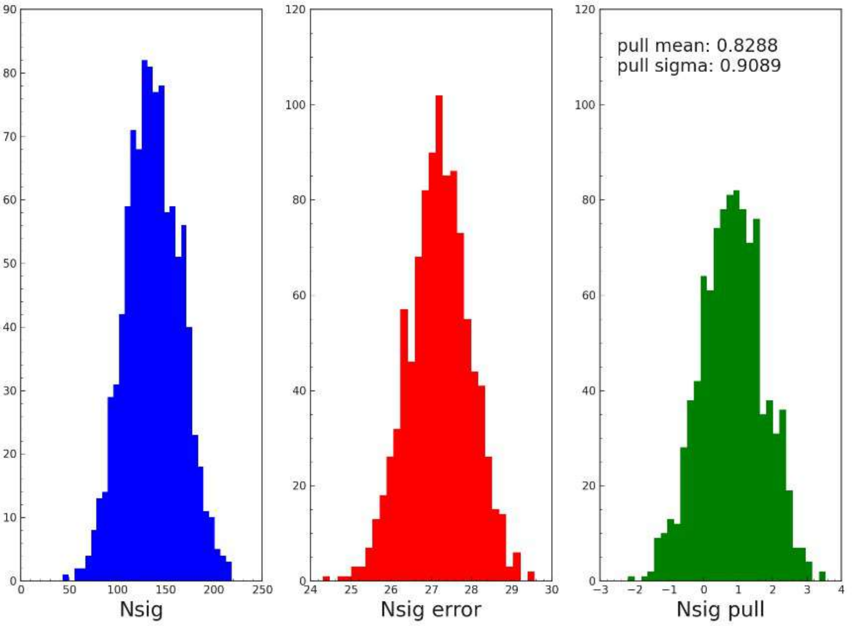

Figure 5.16: Result of the fitter test

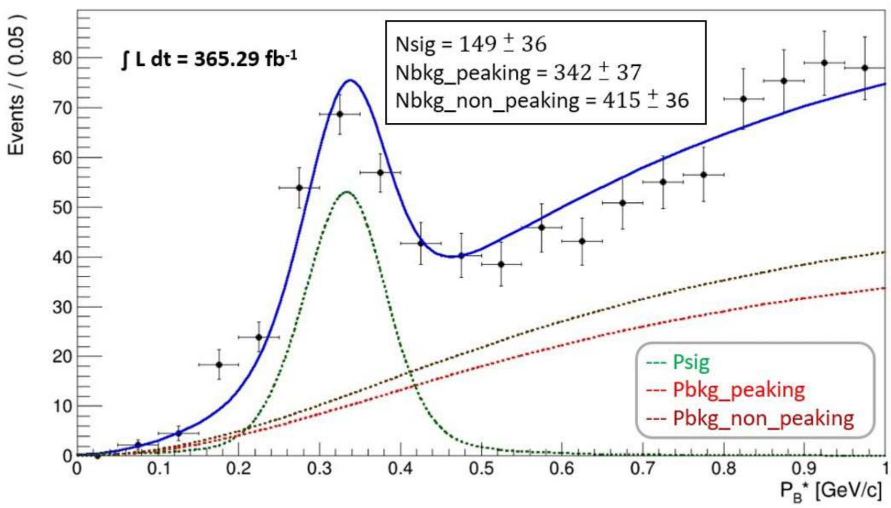

Figure 5.17: Fitting result for signal MC combined with BB background

doi:10.6342/NTU202500482

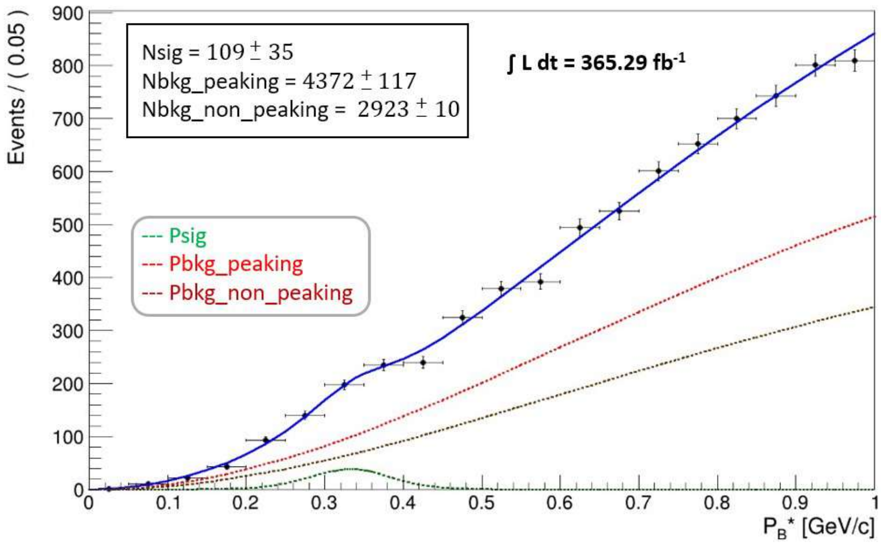

Figure 5.18: Fitting result for signal MC combined with qq background

doi:10.6342/NTU202500482

doi:10.6342/NTU202500482

Chapter 6

Conclusion

Using three-dimensional fit, the signal yields are 137 ± 36 , scaled to the luminosity of the available data $\int$ L dt = 365.29 fb^{-1}. With the accumulation of real data in the future, statistical significance of this result can be further improved.

The pull distribution after fitter test indicates a bias, but it is consistent with the result after a single fit. We have found that this bias arises from the BB background. The two constraints (IP and B mass constraint) we put in reconstruction of our signal B may be the origin of introducing this bias.

doi:10.6342/NTU202500482

doi:10.6342/NTU202500482

Appendix A

Decay Table for the Generation of Signal MC

```
Alias phisig phi

ChargeConj phisig phisig

Decay Upsilon(4S)

1.0 B0sig anti-B0sig B0 anti-B0 VSS_BMIX dm;

Enddecay

Decay B0sig

1.0 phisig K_L0 SSD_CP dm 0.0 1.0 minusTwoBeta 1.0 0.0 1.0 0.0;

Enddecay

CDecay anti-B0sig

Decay phisig

1.0 K+ K- VSS;

Enddecay

End
```


doi:10.6342/NTU202500482

doi:10.6342/NTU202500482

Appendix B

Distribution of Continuum Suppression Training Variables

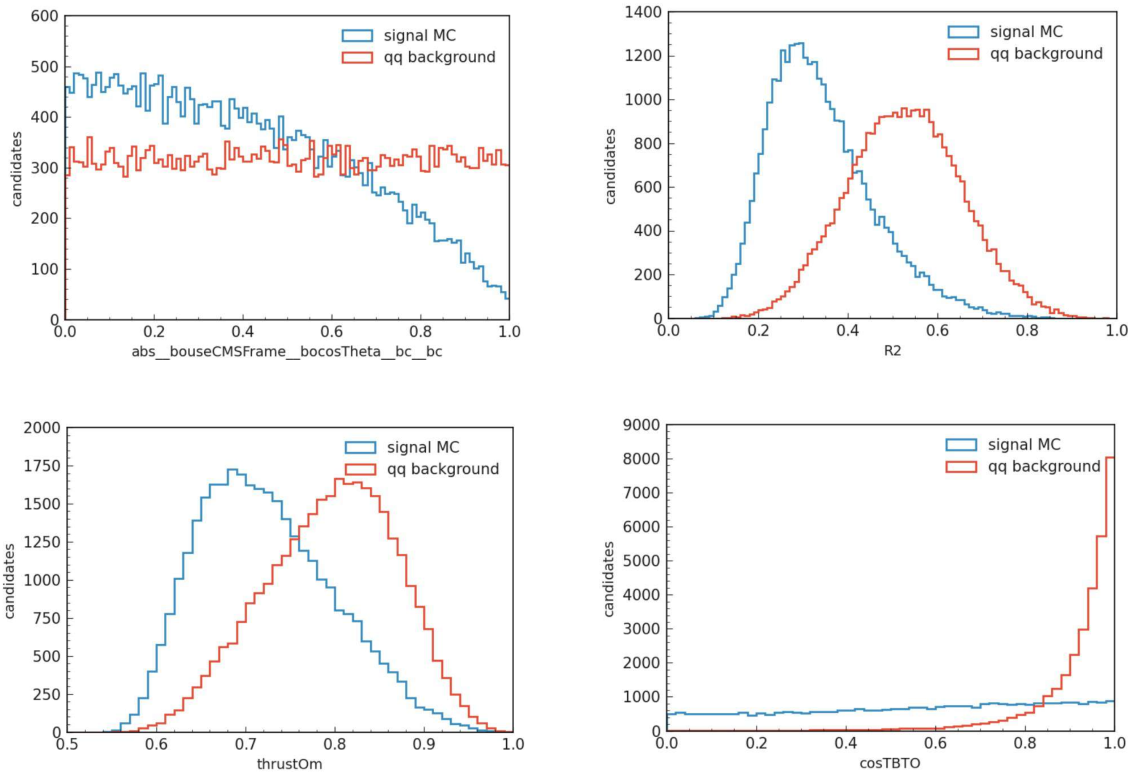

Figure B.1: Distribution of training variables for signal MC and qq background

doi:10.6342/NTU202500482

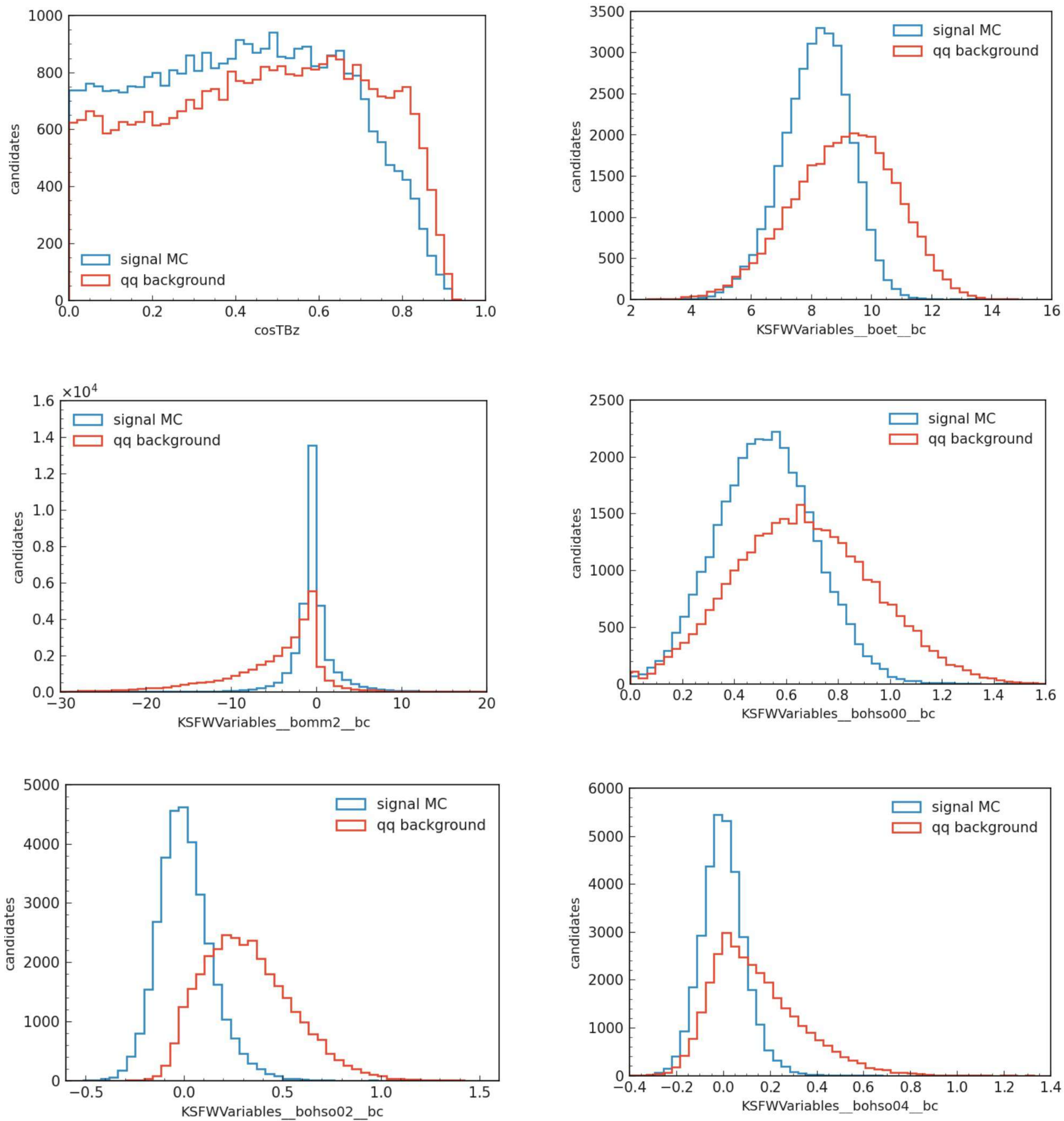

Figure B.2: Distribution of training variables for signal MC and qq background

doi:10.6342/NTU202500482

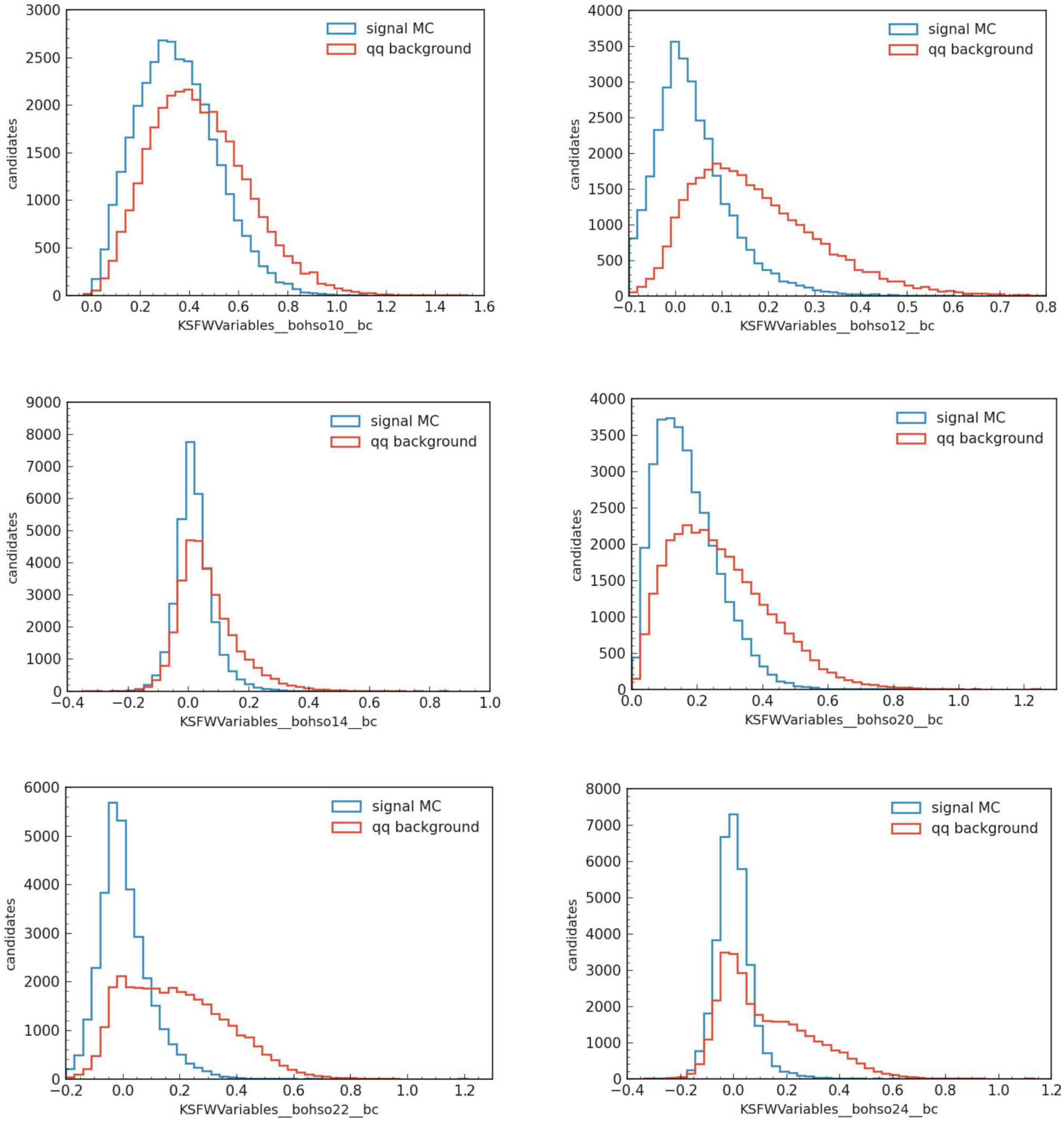

Figure B.3: Distribution of training variables for signal MC and qq background

doi:10.6342/NTU202500482

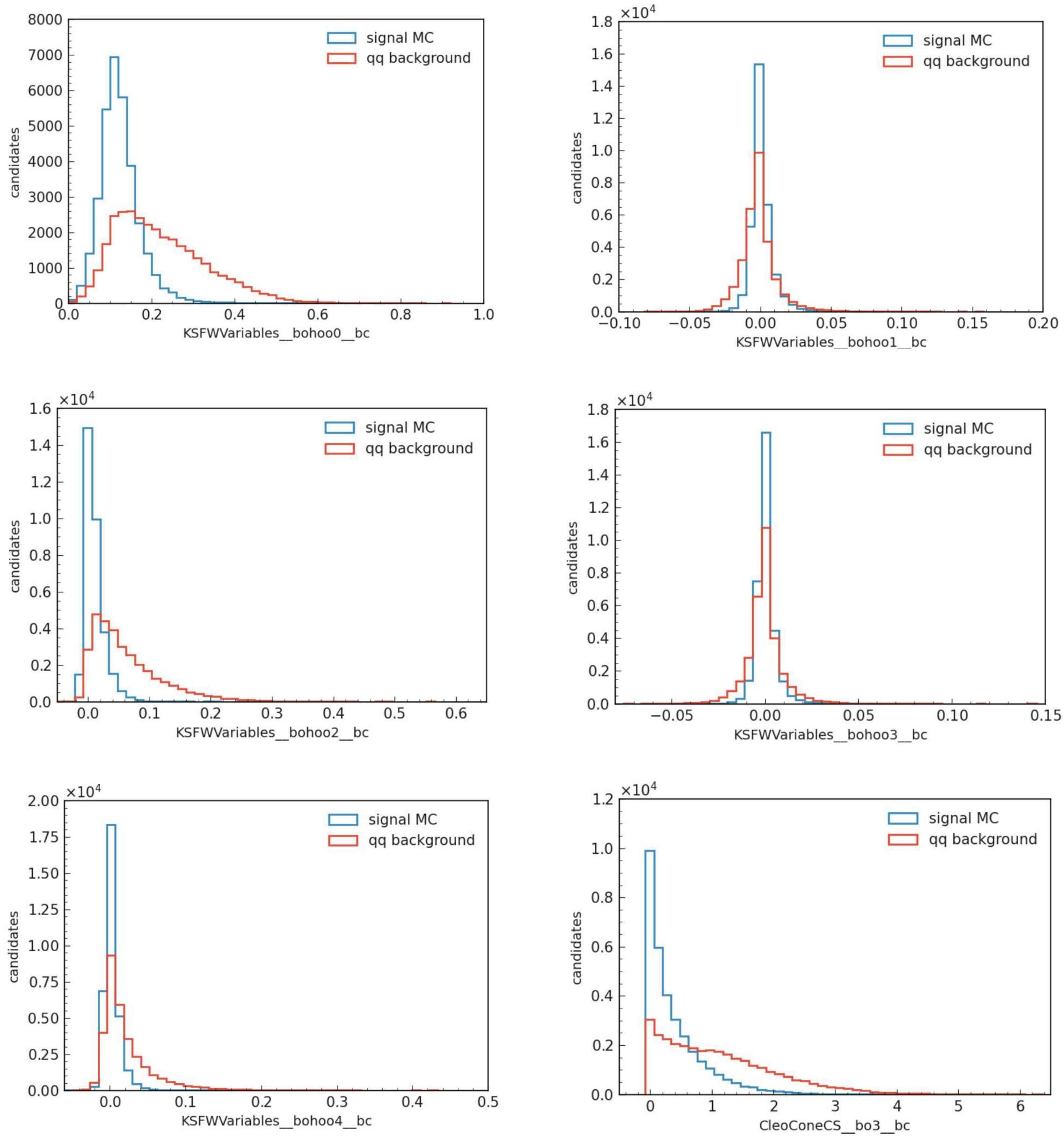

Figure B.4: Distribution of training variables for signal MC and qq background

doi:10.6342/NTU202500482

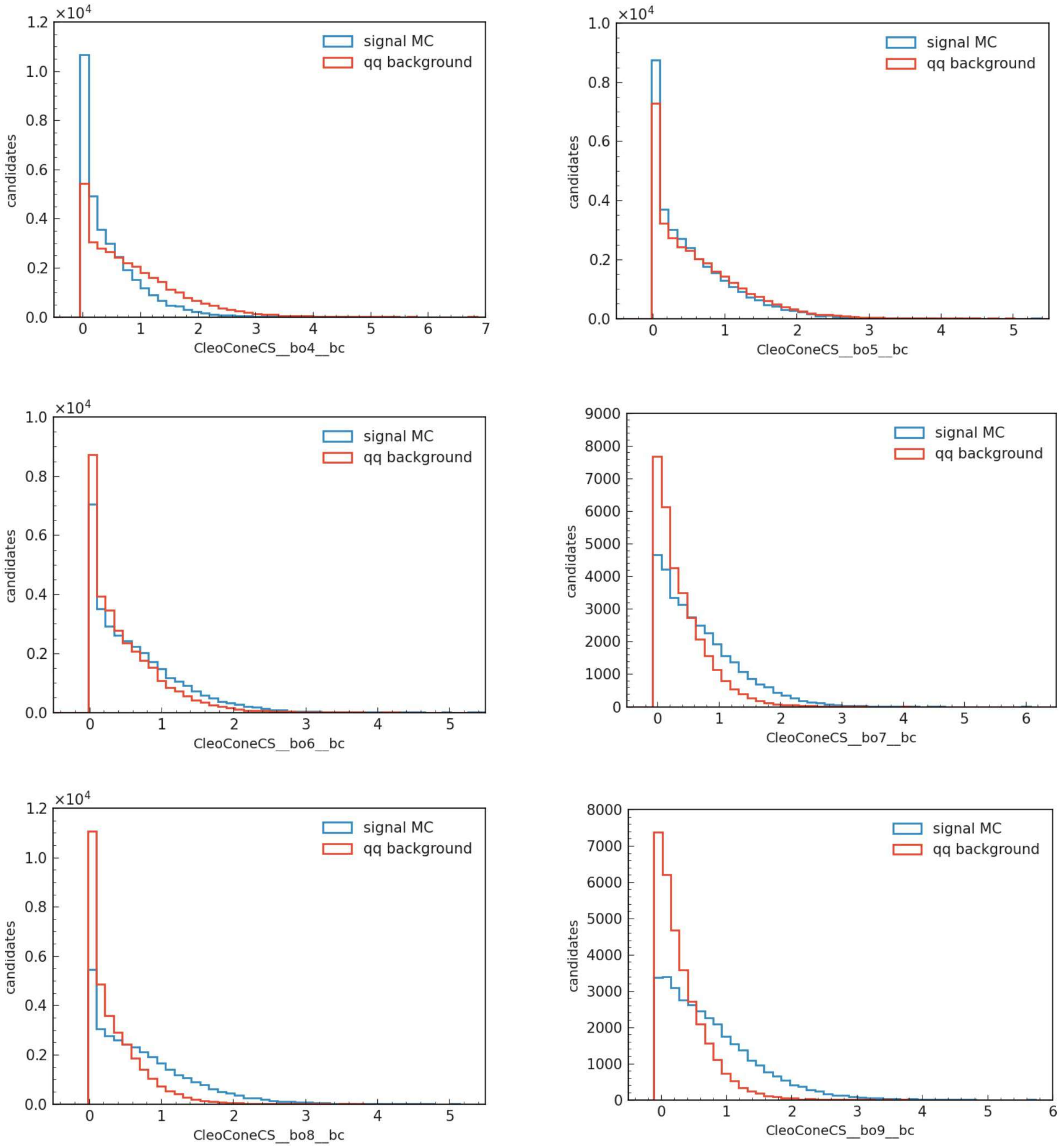

Figure B.5: Distribution of training variables for signal MC and qq background

doi:10.6342/NTU202500482

Appendix B. Distribution of Continuum Suppression Training Variables

doi:10.6342/NTU202500482

Bibliography

[1] B.R.Martion and G.Shaw, *Particle Physics, 4th Edition*, John Wiley & Sons, Ltd, The Atrium, Southern Gate, Chichester, West Sussex, PO19 8SQ, United Kindom, 2017.

[2] M.Thomson, *Modern Particle Physics*, Cambridge University Press, University Printing House, Cambridge CB2 8BS, United Kindom, 2013.

[3] S. Navas *et al.*, *Review of Particle Physics*, Phys. Rev. D **110**, 030001 (2024).

[4] K. F. Chen *et al.*, *Measurement of branching fractions and polarization in B —> phi K(*) decays*, Phys. Rev. Lett. **91**, 201801 (2003).

[5] T. Abe *et al.*, *Belle II Technical Design Report*, KEK-REPORT-2010-1 (2010).

[6] D. J. Lange, *The EvtGen particle decay simulation package*, Nuclear Instruments and Methods in Physics Research Section A: Accelerators, Spectrometers, Detectors and Associated Equipment **462**, 152 (2001), BEAUTY2000, Proceedings of the 7th Int. Conf. on B-Physics at Hadron Machines.

[7] S. Patra and V. Bhardwaj, *MC decay tagging using generated level information with GenMCTagTool*, Technical Report BELLE2-NOTE-TE-2021-002, Belle II, 2021.

[8] J.-H.Su, *Particle Identification of K0L with ECL*, Technical Report BELLE2-NOTE-TE-2024-006, Belle II, 2024.

doi:10.6342/NTU202500482

[9] M. Tanabashi *et al.*, *Review of Particle Physics*, Phys. Rev. D **98**, 030001 (2018).

doi:10.6342/NTU202500482